# The Interaction of Topological Defects in Anisotropically-Elastic Nematic Liquid Crystals

Carter J. Swift
*Macalester College*, cswift@macalester.edu

## Recommended Citation

MACALESTER COLLEGE

# The Interaction of Topological Defects in Anisotropically-Elastic Nematic Liquid Crystals

## Abstract

Topological defects are very well understood so long as the medium in which they exist is isotropically-elastic. They lead to director fields which are easy to calculate and superpose linearly so that a system with any number of defects is analytically treatable. They also have an interaction which is simple in form and can be accurately described by the Peach-Koehler force. In an anisotropically-elastic medium, however, such defects are very poorly understood outside of the single-defect case which was solved by Dzyaloshinskii. In this project, numerical and approximate analytical techniques are applied in order to better understand the interaction between two defects in an anisotropically-elastic medium and how it differs from the well understood isotropically-elastic case.

## Keywords

liquid crystal, topological defect, disclination, free energy

# The Interaction of Topological Defects in Anisotropically-Elastic Nematic Liquid Crystals

**Carter Jefferson Swift**

A thesis submitted in partial fulfillment of the requirements for the degree of

Bachelor of Arts with Honors

Department of Physics and Astronomy

Macalester College

Saint Paul, Minnesota

March 30, 2022

## Abstract

Topological defects are very well understood so long as the medium in which they exist is isotropically-elastic. They lead to director fields which are easy to calculate and superpose linearly so that a system with any number of defects is analytically treatable. They also have an interaction which is simple in form and can be accurately described by the Peach-Koehler force. In an anisotropically-elastic medium, however, such defects are very poorly understood outside of the single-defect case which was solved by Dzyaloshinskii. In this project, numerical and approximate analytical techniques are applied in order to better understand the interaction between two defects in an anisotropically-elastic medium and how it differs from the well-understood isotropically-elastic case.

1

# Contents

# List of Figures

3

4

# Acknowledgement

# 1    Background

## 1.1    Nematic Liquid Crystals

In the field of condensed matter, liquid crystals are considered to be systems which are intermediate between crystals and liquids in terms of symmetry and order. Liquids are entirely symmetric both positionally and orientationally. This is because the constituent particles of a liquid have random distributions of position and orientation, so the system is identical under any translations and rotations. We therefore say that

5

liquids have no order.

In crystals, however, the constituent particles oscillate around lattice sites and have a fixed orientation if they are not spherically symmetric, for example the water molecules in an ice crystal. This heavily restricts the transformations that leave the system invariant, thus the perfect symmetry we see in liquids is broken in crystals. Thus, we say that crystals have both positional and orientational order.

Framing the distinction between liquids and crystals in terms of the presence or absence of these types of order naturally leads one to consider systems where only some order is present. We call such systems liquid crystals. There are, of course, many systems we could imagine that fit this description of having partial order, but for this project we focus on a particular type of system: nematic liquid crystals.

Nematics have orientational order along one axis with no preferred direction on the axis. This is qualitatively similar to magnetic moments aligning in the Ising model, with the important distinction that in nematics if we rotate a particle by 180 degrees to what would be an anti-aligned state in the Ising model, the system is unchanged. We can imagine nematic liquid crystals as describing the behavior of a soup of rod-shaped particles which due to interactions with each other spontaneously align themselves. It is clear, then, that in the nematic phase the lowest energy configuration will feature all particles oriented along the same axis, as depicted in figure 1.

### 1.1.1  Mathematical Description

Nematic liquid crystals can be most completely described mathematically through the nematic order tensor,
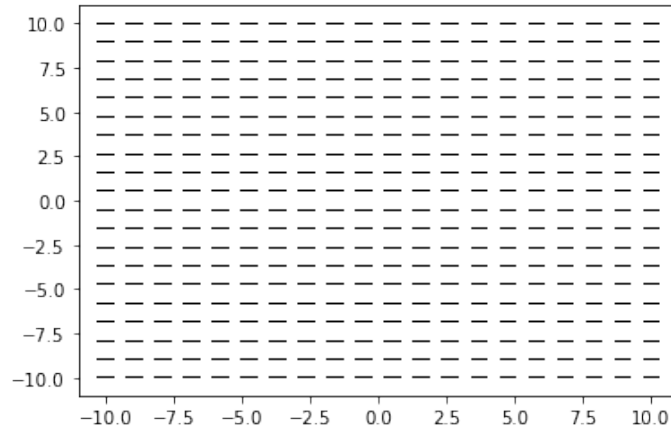
Figure 1: Depiction of a nematic in the uniform configuration

$$Q_{\alpha\beta} = S\left[\frac{3}{2}\mathbf{n}_\alpha\mathbf{n}_\beta - \frac{1}{2}\delta_{\alpha\beta}\right] \tag{1}$$

where $S$ is the scalar order parameter and $\hat{\mathbf{n}}$ is the nematic director [4]. The nematic director, defined up to 180 degree rotations as seen previously, describes locally at each point in the system the direction of nematic order, and the scalar order parameter gives information about how well the particles are aligned with the local director at each point. If we restrict ourselves to the case of perfect nematic order, which physically corresponds to the low-temperature limit where thermal fluctuations are too small to disrupt order, we can assume $S = 1$ everywhere and we may as well work directly with $\hat{\mathbf{n}}$. Since the director is by definition a unit vector, in the two-dimensional case it becomes simpler for many purposes to instead describe the system with $\phi$, the angle the director makes with respect to the positive x-axis.

## 1.2 Elastic Energy

Thus far, we have defined a description for nematics in terms of the director and established that the minimum-energy configuration is one in which all particles are

7

oriented along the same axis, i.e. the director angle is the same everywhere. Naturally, we now want to consider what happens if the director angle is not the same everywhere, that is we want to develop an expression for the elastic energy associated with deviations from the uniform configuration. To do so, we must first consider what form these deviations can take.

### 1.2.1 Distortions

Supposing as before that $\hat{\mathbf{n}}$ is a field defined everywhere and imposing the constraint that $\hat{\mathbf{n}}$ is also continuous and differentiable since sudden changes in the director would be heavily disfavored energetically, we must have that the elastic energy is associated with gradients of the director field. Since the director is a vector, there are unsurprisingly a few ways that these gradients could be oriented with respect to the local average director. We can best intuit what these distinct distortional modes are by considering some examples.

Suppose there is some region in which the director points on average along the x-axis and varies in the x-y plane depending only on the y-coordinate. This gives a behavior that looks like the end of a rope fraying, and this type of distortion is called splay.

Now suppose that the average director is again along the x-axis but we instead vary the director in the plane depending on the x coordinate. This distortion is called bend, and we can picture it as similar to bending a bundle of dry spaghetti.

Finally, consider the same picture again except with the variation depending on the z coordinate (and still acting in the plane). This last type of distortion is called twist, and can perhaps be best visualized as twisting some sort of flat ribbon by its ends.

These are the only three types of distortion possible in three dimensions, though of

8
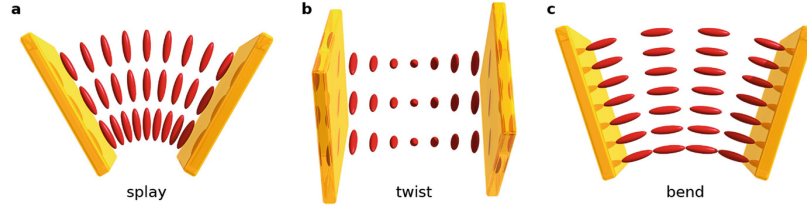
Figure 2: Illustration of the three nematic distortion modes.

course some general distortion can be a linear combination of these three distinct modes. We now can construct expressions for each of these modes of distortion from products of $\hat{\mathbf{n}}$ and the Del operator, $\nabla$. Splay is calculated as $\hat{\mathbf{n}}(\nabla \cdot \hat{\mathbf{n}})$, bend is $\hat{\mathbf{n}} \times (\nabla \times \hat{\mathbf{n}})$, and twist is $\hat{\mathbf{n}} \cdot (\nabla \times \hat{\mathbf{n}})$ [4]. It is notable that the director has to appear twice in each of these formulae to preserve the property of nematics that flipping the director does not change the state.

### 1.2.2 Frank Free Energy

The Frank free energy describes the elastic energy of a nematic in terms of the three modes of distortion. It is given by:

$$G = \iiint \left[ \frac{K_{11}}{2}(\nabla \cdot \hat{\mathbf{n}})^2 + \frac{K_{22}}{2}(\hat{\mathbf{n}} \cdot (\nabla \times \hat{\mathbf{n}}))^2 + \frac{K_{33}}{2}|\hat{\mathbf{n}} \times (\nabla \times \hat{\mathbf{n}})|^2 \right] d^3x \quad (2)$$

Each of the three terms in the above equation is of the form $\frac{k}{2}(\text{distortion})^2$, perhaps unsurprisingly reminiscent of the equation for the energy of a spring, $\frac{k}{2}x^2$ since that too describes a system that resists distortion, albeit in a much simpler scenario. Further, each of the distortion modes has its own associated elastic constant $K_{ii}$. In principle some arbitrarily specified particle-particle interaction could be much more sensitive to one type of distortion than another, so in general the three modes of distortion will contribute differently to the total elastic energy.

9

Now, restricting the system to two dimensions the twist term disappears, leaving us with just the splay and bend terms.

$$G_{2D} = \iint \left[ \frac{K_{11}}{2}(\nabla \cdot \hat{\mathbf{n}})^2 + \frac{K_{33}}{2}|\hat{\mathbf{n}} \times (\nabla \times \hat{\mathbf{n}})|^2 \right] d^2x \qquad (3)$$

Since the most interesting behavior of a nematic will depend on the relationship between the two elastic constants and not on their overall magnitude, it is convenient to now reexpress equation 3, substituting $K = \frac{K_{11}+K_{33}}{2}$ and $\epsilon = \frac{K_{11}-K_{33}}{K_{11}+K_{33}}$:

$$G_{2D} = \frac{K}{2} \iint \left[ (1+\epsilon)(\nabla \cdot \hat{\mathbf{n}})^2 + (1-\epsilon)|\hat{\mathbf{n}} \times (\nabla \times \hat{\mathbf{n}})|^2 \right] d^2x \qquad (4)$$

$K$ is the overall elastic constant, and we can generally neglect it as unimportant to the behavior of the system (assuming the low-temperature limit henceforth), more technically choosing our units always such that $\frac{K}{2} = 1$. $\epsilon$ we refer to as the elastic anisotropy, a dimensionless parameter dictating how different the bend and splay constants are. If both modes of distortion contribute equally to the elastic energy, $\epsilon = 0$ and we say we are in the isotropically-elastic case. All other values of $\epsilon$ correspond to elastically anisotropic systems, with values approaching 1 indicating that the contribution from bend will be very small compared with the contribution from splay, and values approaching $-1$ indicating the opposite.

## 1.3    Topological Defects

In previous sections we established that the minimum-energy configuration of a nematic is a uniform configuration, e.g. $\phi = 0$ everywhere, and that any deviation from this configuration results in a higher free energy and is thus disfavored. One would

10

naively conclude from this that any nematic system will always be in a uniform configuration, barring thermal fluctuations, but it turns out that this is very much not the case.

Much as random seeding gives rise to defects in ordinary crystals, the condensation into a nematic phase from an initial isotropic phase where all particles are oriented randomly can also cause defects. These defects in a nematic are disclinations, the orientational equivalent to a dislocation in an ordinary crystal, and they have the property of being topologically protected, so they are also referred to as topological defects. This topological protection formally means that there is no continuous transformation from a defected configuration to the uniform configuration, and so defects are stable. Physically, this means that defected configurations are very deep local minima of the free energy where the only escape is to input enough energy to the system to completely lift the defected region out of the nematic phase before letting it recondense into a uniform configuration.

We must now consider exactly what form this topological protection takes. That is, we must determine a quantity of a nematic configuration which is conserved under continuous transformations of the director field. This conserved quantity will then be the topological invariant associated with disclinations.

To find this quantity, consider generally what a defect could look like in a nematic: there will be some point around which the director angle $\phi$ changes as a function of $\theta$, where $\theta$ is the polar angle treating the defect point as the origin. There is an additional constraint, which is that $\phi$ must be continuous, i.e. $\phi(0) = \phi(2\pi)$. Coupled with the nematic property that $\phi + \pi = \phi$, we can arrive at some hypothetical defect of the form $\phi(\theta) = \frac{n}{2}\theta$ where $n$ is an integer. We will see shortly that this is indeed the form a defect takes in the isotropically-elastic case.

11
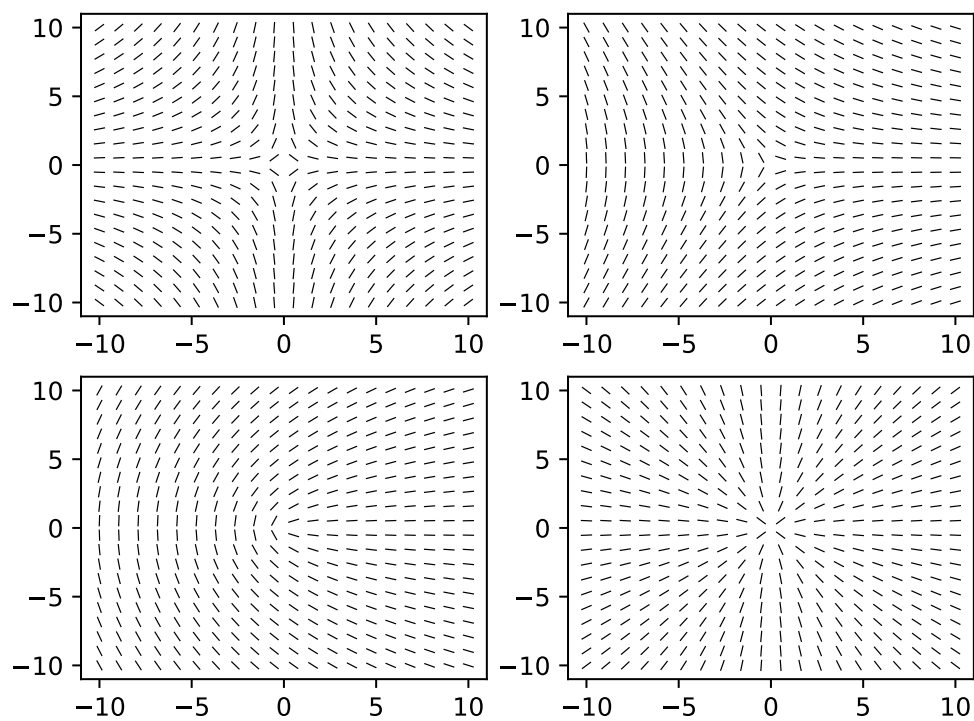
Figure 3: Illustrations of topological defects of charges -1,-1/2,1/2, and 1, reading respectively from top left to bottom right.

12

Now, a sensible way to describe such a defect with a scalar quantity would be the total rotation of the director around a loop enclosing the defect. Such a loop is called a Burgers Circuit, and the resulting quantity is called the topological charge, defined as follows [4]:

$$q_{enclosed} = \frac{1}{2*\pi} \oint d\phi \tag{5}$$

This definition is reminiscent of Gauss' Law for electrostatics, highlighting a helpful qualitative picture of topological defects as being similar to charged particles, albeit with important differences when examined in detail.

For our above example, the topological charge given by Eq. 5 is $\frac{n}{2}$. In theory, a defect could exist with $n$ equal to any integer, positive or negative, however such defects would in practice generally not be stable. This is because only the total topological charge in a system is conserved, so defect cores with a large charge will generally split into multiple defect cores with smaller charges. In another parallel with electrostatics, like-charge defects will repel each other while opposite-charge defects will attract each other and annihilate. The splitting of defect cores can be viewed as a manifestation of this like-charge repelling property and results in only the lowest-charge defects being of much relevance.

### 1.3.1   Isotropically-Elastic Case

Let us now see how the specific geometry of a disclination arises from its topological properties coupled with the minimization of the Frank free energy.

In the isotropically-elastic case, the terms in Eq. 4 combine, reducing dramatically

13

to

$$G = \frac{k}{2} \iint |\nabla \phi|^2 d^2 x \tag{6}$$

where we have also switched to using the director angle directly.

Finding the minimum configuration then can be converted into a differential equation, i.e. the Euler-Lagrange equation, which yields the following relation:

$$\nabla^2 \phi = 0 \tag{7}$$

We then see that the earlier presumed form of a topological defect satisfies this equation and is thus the minimum-energy form of a defect in an isotropically-elastic medium.

### 1.3.2 Anisotropically-Elastic Case

When the medium is no longer taken to be isotropically-elastic, the calculation becomes significantly more involved, though it is still possible to find analytically the field of a single defect.

We begin from Eq. 4, but now expand the operators and the director explicitly in polar coordinates. In doing so, we note that the director field should be independent of the radial coordinate, only depending on $\theta$. This yields

$$G = \frac{k}{2r^2} \iint \left( \frac{\partial \phi}{\partial \theta} \right)^2 (1 + \epsilon \cos(2(\phi - \theta))) d^2 x. \tag{8}$$

Then, finding the Euler-Lagrange equation as we did previously for the isotropically-

14

elastic case gives us

$$0 = \frac{\partial^2 \phi}{\partial \theta^2}(1 + \epsilon \cos 2(\phi - \theta)) + \left(2\frac{\partial \phi}{\partial \theta} - \left(\frac{\partial \phi}{\partial \theta}\right)^2\right) \epsilon \sin 2(\phi - \theta). \tag{9}$$

Equation 9 is still not so straightforward to solve, being second-order and nonlinear. Fortunately, a solution was found by Dzyaloshinskii [2], given by

$$\theta = p \int_0^{\phi - \theta} \left[\frac{1 + \epsilon \cos 2x}{1 + p^2 \epsilon \cos 2x}\right]^{1/2} dx \tag{10}$$

where $p$ is itself given by solving

$$\pi = (q - 1)p \int_0^{\pi} \left[\frac{1 + \epsilon \cos 2x}{1 + p^2 \epsilon \cos 2x}\right]^{1/2} dx. \tag{11}$$

This solution is clearly not particularly easy to work with, as it involves first solving for $p$ via an integration that must be done numerically, then solving for $\phi$ once the $\theta$ associated with a certain difference $\phi - \theta$ is found by integrating again.



(a) $\epsilon = -0.5$        (b) $\epsilon = 0.5$
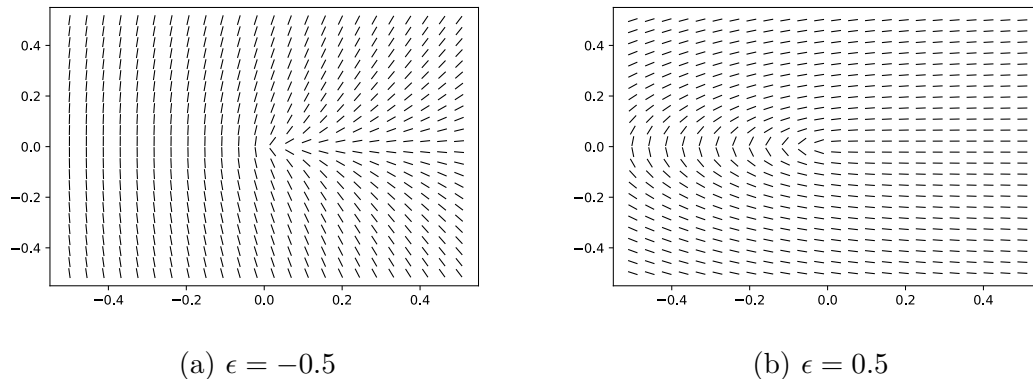
Figure 4: Illustrations of a 1/2 defect in anisotropically elastic media.

While this full solution is important in the numerical work, in order to have a point

15

of comparison for our analytic approximations for small $\epsilon$, we want to similarly find the first-order in epsilon component of the Dzyaloshinskii solution.

To do so, we simply assume that $\phi$ is of the form

$$\phi = q\theta + \epsilon C \sin(2(1-q)\theta) + \ldots$$

and plug into Eq. 9, neglecting higher powers of $\epsilon$ and solving to fix the constant and obtain the solution

$$\phi_{DZ} \approx q\theta - \frac{\epsilon}{4}\frac{q(2-q)}{(1-q)^2}\sin(2(1-q)\theta). \tag{12}$$

## 1.4 Interacting Defects

Thus far we have discussed only systems with a single defect, but of much more interest are systems containing two defects interacting with each other. As we show later on, studying this interaction is not straightforward in the anisotropically-elastic case since the Euler-Lagrange equation is nonlinear. In the isotropically-elastic case, though, we can simply take the director field to be a superposition of the individual director fields of two defects. This then allows us to calculate the interaction energy and thus the inter-defect force in one of two ways.

The first and most obvious way is to directly integrate the free-energy. In [1] this is done via a surface integral around each defect after introducing cuts along the discontinuity where $\phi$ jumps from $-\pi$ to $\pi$. The result, also obtained in [4] via a

16

different integration approach is:

$$E_{int} = 2\pi k q_1 q_2 \ln(\frac{a}{d}) \tag{13}$$

where $a$ is the radius of the defect cores and $d$ is the separation between the defects. Thus, oppositely-charged defects indeed attract similarly to electrostatic charges, with a similar $\ln(d)$ potential as in 2D electrostatics (although different to the $\frac{1}{d}$ potentials of 3D electrostatics). This in turn tells us that the force scales as $\frac{1}{d}$.

The other, more elegant way to find the interaction is via the Peach-Koehler force. Originally developed for dislocations in ordinary crystals, this approach relies on the linearity of the medium. It treats the interaction as the response of one defect to the "effective stress" induced at its location by the other defect [3].

Formally,

$$\mathbf{f}_{PK} = (\sigma \cdot \mathbf{b}) \times \hat{z}$$

where in 2D the important components of $\sigma$ are given by

$$\sigma_{zi} = \partial_i \phi$$

and $\mathbf{b}$ is the effective Burgers vector, given by $\mathbf{b} = 2\pi q \hat{z}$. Computing the Peach-Koehler force using the isotropic defect solutions reproduces the above result of a force which scales as $\frac{1}{d}$ and is attractive for oppositely-charged defects. Further, the force found is equal and opposite when exchanging which defect we view as the one being acted upon by the stress of the other, which we should expect from Newton's third law, and is a good check of the validity of this approach.

17

# 2 Methods

While the isotropically-elastic case could be analyzed exactly for two defects and the anisotropically-elastic case yielded the semi-analytic Dzyaloshinskii solution for a single defect, it is not possible to find an exact analytic solution for the two defect anisotropically-elastic case.

In order to probe the structure and behavior of the director field under these circumstances, numerical and approximate analytic methods were used in conjunction to understand the nearly-isotropic regime ($|\epsilon| \lessgtr 0.15$). The numerical methods can also be readily applied to the regime of high elastic anisotropy.

This section will first describe the derivation of the differential equation which the minimum-energy director field must satisfy, then will address specifically the numeric and analytic techniques used in finding solutions.

## 2.1 Director Field Equation

Starting from Eq. 4, we want to derive the differential equation describing the minimum-energy director field for a general configuration of defects. Unlike when deriving the equation that yielded the Dzyaloshinskii solution, we can no longer make the assumption that the director angle is independent of $r$. Indeed, brief consideration reveals that it is no longer convenient to use polar coordinates when multiple defects are present, so we first write the free energy density explicitly in cartesian coordinates, using also the fact that $\hat{n} = \cos\phi\hat{x} + \sin\phi\hat{y}$:

$$g = \frac{k}{2}\left[(1+\epsilon)(\phi_y\cos\phi - \phi_x\sin\phi)^2 + (1-\epsilon)(\phi_x\cos\phi + \phi_y\sin\phi)^2\right] \qquad (14)$$

18

Where $\phi_x$ and $\phi_y$ refer to the derivatives of $\phi$ with respect to the subscripted coordinate.

From this, we must find the Euler-Lagrange equation according to the following:

$$\frac{\partial g}{\partial \phi} - \frac{\partial}{\partial x}\frac{\partial g}{\partial \phi_x} - \frac{\partial}{\partial y}\frac{\partial g}{\partial \phi_y} = 0 \tag{15}$$

We calculate each of these terms separately:

$$\frac{\partial g}{\partial \phi} = -2\cos(2\phi)\phi_x\phi_y + \epsilon\sin(2\phi)(\phi_x^2 + \phi_y^2),$$

$$\frac{\partial}{\partial x}\frac{\partial g}{\partial \phi_x} = \frac{\partial}{\partial x}\left[2\phi_x(1 - \epsilon\cos 2\phi) - 2\epsilon\sin(2\phi)\phi_y\right]$$

$$= 2(\phi_{xx}(1 - \epsilon\cos 2\phi) - \epsilon\sin(2\phi)\phi_{xy} + 2\epsilon\sin(2\phi)\phi_x^2 - 2\epsilon\cos(2\phi)\phi_x\phi_y),$$

$$\frac{\partial}{\partial y}\frac{\partial g}{\partial \phi_y} = \frac{\partial}{\partial y}\left[2\phi_y(1 + \epsilon\cos 2\phi) - 2\epsilon\sin(2\phi)\phi_x\right]$$

$$= 2(\phi_{yy}(1 + \epsilon\cos 2\phi) - \epsilon\sin(2\phi)\phi_{xy} - 2\epsilon\sin(2\phi)\phi_y^2 - 2\epsilon\cos(2\phi)\phi_x\phi_y).$$

Combining these components together yields the differential equation:

$$\nabla^2\phi + \epsilon\left[\sin 2\phi(\phi_x^2 - \phi_y^2 - 2\phi_{xy}) + \cos 2\phi(\phi_{yy} - \phi_{xx} - 2\phi_x\phi_y)\right] = 0 \tag{16}$$

19

Computing the minimum-energy defect configuration has now been reduced to solving this differential equation. This is progress, though it quickly becomes clear that there is little hope of solving the problem analytically. Thus, we turn to a combination of numerical and approximate analytical methods in order to find solutions and understand the important behavior.

## 2.2 Numerical Approach

The director field equation derived above is a nonlinear, second-order partial differential equation. In order to solve this equation, we deemed a finite-difference relaxation method with Neumann boundary conditions to be suitable. This choice of Neumann boundary conditions is physically reasonable so long as no defects are particularly close to the boundary and the total topological charge inside the system is 0. Since we are interested in probing the interaction between $+\frac{1}{2}$ and $-\frac{1}{2}$ defects, this assumption is satisfied so long as the system size is chosen to be large compared to the defect separation. Generally, we took the system size to be 1000 by 1000, restricting the range of separations we studied to not put defects too close to the boundary

To solve, we begin by defining a square grid of director angles indexed by $i, j$ which will after the computation contain the numerical approximation to the minimum-energy director angle field. Proper initialization of the angles is required both to allow convergence of the algorithm and to allow us to enforce that the two defects are present where desired.

Fortunately, we have the exact Dzyaloshinskii solution for a single anisotropically-elastic defect, so we take the initial configuration to be the sum of two Dzyaloshinskii solutions, one centered at each of the defect positions. To ensure that the defects are fixed in place, we define a region of some small radius around each defect to be the

20

defect core in which the director field is simply initialized to the correct Dzyaloshinskii solution for that defect and left unchanged by the solution algorithm. We know this to be an approximately correct approach so long as the core radius is small compared to the defect separation, as shown via the analytic approach we take in section 2.3.

Next, we substitute all derivatives in Eq. 16 with their respective finite-difference approximations, derived from taylor series expansions around a point. Centered differences were used predominantly due to their improved accuracy compared to one-sided differences, though along the boundaries such one-sided differences had to be used for first derivatives. This is due to our choice of Neumann boundary conditions requiring first derivatives to be calculated at the boundary where the centered difference is of course undefined.

Now, having discretized both our system and the differential equation, we are ready to begin the process of solving. We repeatedly iterate through the array of director angles, at each point updating the angle $\phi_{ij}$ by locally solving the discretized differential equation using the surrounding eight angles as inputs. Provided we have chosen an initial configuration sufficiently close to the minimum-energy configuration, this scheme should hopefully converge after some number of iterations according to an appropriate stopping criterion.

For our stopping criterion, we define a way to determine how far a given configuration is from the minimum energy configuration. We know that the minimum-energy configuration satisfies the differential equation everywhere, so after each iteration we compute the LHS of the differential equation at each lattice point and keep track of the maximum absolute value we encounter. This quantity will be zero (up to some discretization error) for the minimum-energy configuration, so we choose a tolerance and stop the algorithm when the maximum absolute deviation is less than the cho-

21
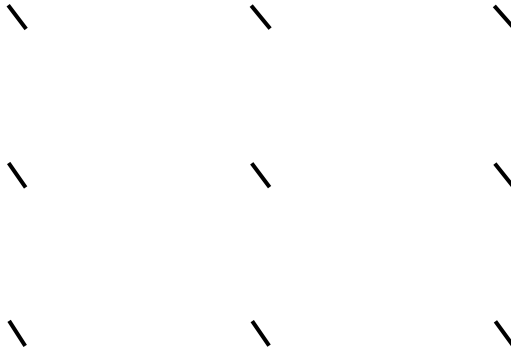
Figure 5: Illustration of a sample calculation neighborhood for the relaxation method. The middle angle is updated according to the 8 surrounding angles.

sen tolerance. This way, when the stopping criterion is satisfied we can be confident that the resulting director field is an accurate representation of the minimum-energy configuration at each point.

In practice, we found that the convergence of the algorithm was not always stable. It would often converge quickly to some relatively small minimum then diverge rather slowly away from it. Thus we often had to choose the stopping criterion to be whatever minimum could be reached with the method rather than setting it arbitrarily small.

The algorithm as described so far is nearly complete, however there remains a major flaw that caused significant issues in our earliest numerical results. This flaw, as we discovered, has to do with a failure to take into account the key property of nematics: their symmetry under 180 degree rotations of any local director.

Looking back at the differential equation explicit derivatives of the director angle appear, so we can begin to understand the problem by considering what occurs at the edges of the angular domain. The $\pi$ radian rotation induced by each defect unavoidably guarantees that there is a line of lattice points where, for example, an angle slightly above 0 radians is directly adjacent to an angle slightly below $\pi$ ra-

22

dians. Physically we understand that the derivative of $\phi$ across this line should be fairly small. Numerically, however, we will obtain a large derivative because 0 is not mathematically equal to $\pi$, effectively creating a discontinuity where there should be none.

This may seem to be a very fundamental issue with our approach, but fortunately there is a reasonably simple albeit somewhat inelegant workaround. There is always guaranteed to be a discontinuity at the boundaries of the angular domain, but we are not forced to use the same angular domain for each calculation. Instead, we devise a way to dynamically adjust the domain depending on the local average director angle.

In any neighborhood of adjacent lattice points, $\phi$ varies relatively little, so we can always find a domain that shifts the discontinuity away from the angles we are currently calculating with. By doing so, we resolve the issue and complete the algorithm.

## 2.3    Approximate Analytic Approach

Starting again from Eq. 16, we want to identify a regime in which we can make some analytical progress. An obvious choice, and the one we decided to investigate, is the regime in which $\epsilon$ is small. As we have the exact solution for $\epsilon = 0$, we can hope to make progress via a perturbative method.

Specifically, we suppose that the solution $\phi$ can be expanded in terms which are proportional to powers of $\epsilon$:

$$\phi = \phi_{iso} + \epsilon\phi_c + \epsilon^2\phi_{c2} + \ldots \tag{17}$$

In principle we can include as many terms as we wish, however for simplicity we

23

restrict ourselves to only the first-order correction, which should capture most of the important behavior in the small $\epsilon$ limit.

We now substitute the expanded expression for $\phi$ into Eq. 16, working through a great deal of algebra and neglecting higher-than-linear powers of $\epsilon$ to obtain the following:

$$\nabla^2 \phi_c = \frac{q_1(2 - q_1)\epsilon}{r_1^2} \sin\left(2(1 - q_1)\theta_1 - 2q_2\theta_2\right) \tag{18}$$
$$+ \frac{q_2(2 - q_2)\epsilon}{r_2^2} \sin\left(2(1 - q_2)\theta_2 - 2q_1\theta_1\right)$$
$$- \frac{2\epsilon q_1 q_2}{r_1 r_2} \sin\left((1 - 2q_1)\theta_1 + (1 - 2q_2)\theta_2\right)$$

This expression is as expected somewhat simpler than our starting point. However, it still resists analytic solution, so we need to make further approximations in order to understand its behavior. We now will take limits of the defect separation in order to determine the structure of the director field in various regions. The three regions we can investigate this way are: far from both defects compared to the defect separation $d$, close to one defect compared to $d$, and midway between the defects in a region which is small compared to $d$.

Each of the expressions we find will have some radial dependence which follows from the order of terms we choose to keep, as well as an angular dependence which is the more qualitatively important part of the solution. We will later compare the angular components against the numerical results.

### 2.3.1   Far From Both Defects

The first limit we take is that the distance from the origin to the test point, $r$, is much larger than the defect separation $d$. Neither of these parameters appears explicitly in

Eq. 18, so the first order of business is in transforming to a polar coordinate system with the origin at the midpoint between the two defects. This will allow us to write $r_1, r_2, \theta_1, \theta_2$ in terms of $r$ and $\theta$, expressions which we can then expand in orders of the small quantity $\frac{d}{r}$.
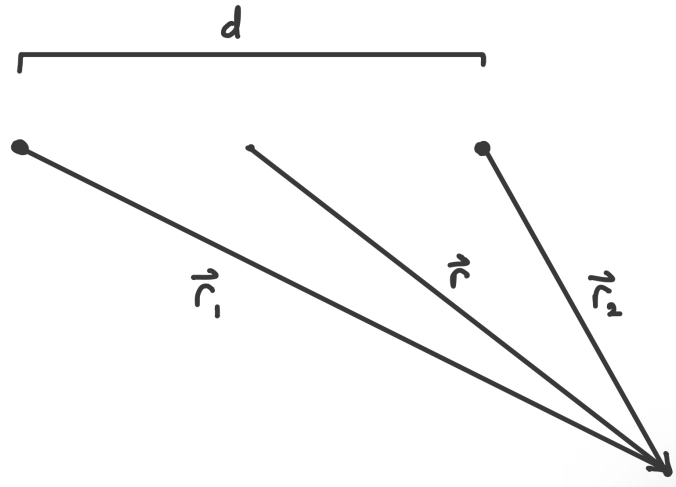


Figure 6: Geometric picture of the regime $d \ll r$

According to the geometry in Fig. 6, we can write the quantities as follows:

$$\frac{1}{r_1} = \frac{1}{\sqrt{r^2 + (\frac{d}{2})^2 + rd\cos\theta}}$$

$$\sin\theta_1 = \frac{r\sin\theta}{\sqrt{r^2 + (\frac{d}{2})^2 + rd\cos\theta}}$$

$$\cos\theta_1 = \frac{\frac{d}{2} + r\cos\theta}{\sqrt{r^2 + (\frac{d}{2})^2 + rd\cos\theta}}$$

The similar quantities associated with defect 2 are not explicitly written here because they are nearly identical to the above, with just a few differences of sign.

Now we factor out powers of $r$ in order to obtain expressions that are written in terms of $\frac{d}{r}$, then we replace the resulting expressions with taylor series approximations which

25

are first order in $\frac{d}{r}$, yielding the following:

$$\frac{1}{r_1} \approx \frac{1}{r}\left(1 - \frac{1}{2}\frac{d}{r}\cos\theta\right)$$

$$\sin\theta_1 \approx \sin\theta\left(1 - \frac{1}{2}\frac{d}{r}\cos\theta\right)$$

$$\cos\theta_1 \approx \cos\theta + \frac{1}{2}\frac{d}{r}\sin^2\theta$$

As mentioned above, we obtain roughly similar results for the quantities associated with the defect 2 coordinates. In order to plug in the angular expressions, we first need to rewrite the sines which appear in Eq. 18. Without much loss of generality, we choose defect 1 to be the negative defect so that we can properly expand the sines. The opposite choice would also be appropriate and would yield a result with very similar behavior.

Examining the first term, we obtain

$$\sin(3\theta_1 - \theta_2) = \cos\theta_2(3\sin\theta_1 - 4\sin^3\theta_1) + \sin\theta_2(3\cos\theta_1 - 4\cos^3\theta_1)$$
$$\approx \sin 2\theta + \frac{d}{r}(\sin\theta - \sin 3\theta) \tag{19}$$

For the second term we get

$$\sin(\theta_1 + \theta_2) = \sin\theta_1\cos\theta_2 + \cos\theta_1\sin\theta_2$$
$$\approx \sin 2\theta \tag{20}$$

26

And for the third term we find

$$\sin 2\theta_1 = 2 \sin \theta_1 \cos \theta_1$$

$$\approx \sin(2\theta) - \frac{1}{2}\frac{d}{r}\left(\sin\theta - \sin 3\theta\right) \tag{21}$$

Now we simply combine these angular terms with the rest of the equation and neglect higher powers of $\frac{d}{r}$ where they appear to arrive at the final differential equation

$$\nabla^2 \phi_c = -\frac{\epsilon}{2}\frac{d}{r^3}\left[\sin\theta - 5\sin 3\theta\right] \tag{22}$$

This equation is quite simple, and we can guess the form of the solution with knowledge of how the Laplacian operator acts in polar coordinates:

$$\phi_c = \frac{d}{r}\epsilon(A\theta\cos\theta + B\sin 3\theta) \tag{23}$$

Plugging this ansatz into the equation, we obtain the coefficients A and B, and can then write the solution as:

$$\phi_c = \frac{d\epsilon}{2r}\left[\frac{1}{2}\theta\cos\theta - \frac{5}{9}\sin 3\theta\right] \tag{24}$$

An important caveat to the solution we have just derived is that it only captures the anisotropically-elastic behavior of the defects. There is also of course an influence from the isotropically-elastic components of the defect fields, and we need to obtain a description of these components to finish our treatment of this region.

We do so by expanding the isotropic component w.r.t the same small parameter as

27

throughout this section:

$$\phi_{1,iso} = q_1\theta_1 = q_1 \arctan\left(\frac{\sin\theta_1}{\cos\theta_1}\right) \approx q_1 \arctan\left(2\frac{d}{r}\sin\theta\right) \approx 2q_1\frac{d}{r}\sin\theta \qquad (25)$$

For defect 2, we similarly obtain

$$\phi_{2,iso} \approx -2q_2\frac{d}{r}\sin\theta \qquad (26)$$

### 2.3.2 Midway Between Defects

Now we want to consider the director field in a small region around the midpoint between the two defects. The setup for this case is identical to that of the previous section, we simply take the opposite limit, that is $\frac{r}{d} \ll 1$.
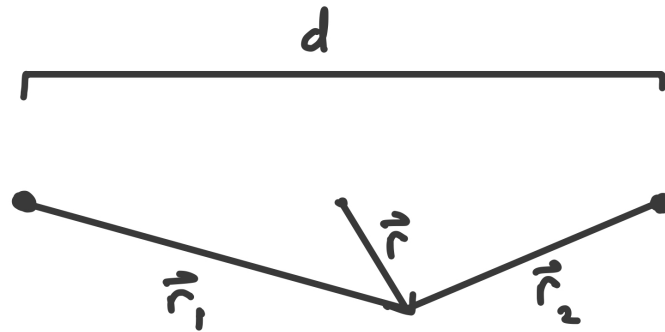


Figure 7: Geometric picture of the regime $r \ll d$ expanded near the origin

After changing coordinates and applying our approximation we get for the quantities associated with defect 1:

$$\frac{1}{r_1} \approx \frac{2}{d}\left(1 - 2\frac{r}{d}\cos\theta\right)$$

$$\sin\theta_1 \approx 2\frac{r}{d}\sin\theta$$

$$\cos\theta_1 \approx 1$$

28

and as before the similar quantities for defect 2 are nearly identical, but with some signs flipped. We now examine the three sines appearing in Eq. 18 separately, finding:

$$\sin(3\theta_1 - \theta_2) \approx -6\frac{r}{d}\sin\theta + 6\frac{r}{d}\sin\theta = 0$$

$$\sin(\theta_1 + \theta_2) \approx -2\frac{r}{d}\sin\theta + 2\frac{r}{d}\sin\theta = 0$$

$$\sin(2\theta_1) \approx 4\frac{r}{d}\sin\theta$$

We see that already by approximating the sines we have reduced the equation down to a single term. Writing the new equation out, we find

$$\nabla^2\phi_c = 8\epsilon\frac{r}{d^3}\sin\theta \tag{27}$$

which we can easily solve to find

$$\phi_c = \epsilon\frac{r^3}{d^3}\sin\theta \tag{28}$$

As in the previous case, we add the two isotropic corrections as well, which in this case are proportional to $\frac{r}{d}$ but otherwise exactly match those from before.

These three corrections together give us the complete picture of the director field close to the midpoint of the two defects.

29

### 2.3.3 Close to One Defect

The final region that we are interested in finding the approximate director field in is the region close to one defect or the other with respect to the defect separation. Formally, this corresponds to the limit $\frac{r}{d} \ll 1$, just as in the previous section. The key difference here is that instead of working in coordinates centered at the midpoint between the defects, we work with the coordinates of defect 1, rewriting $r_2$ and $\theta_2$ in terms of $r_1$, $\theta_1$, and $d$ before expanding in the small parameter.
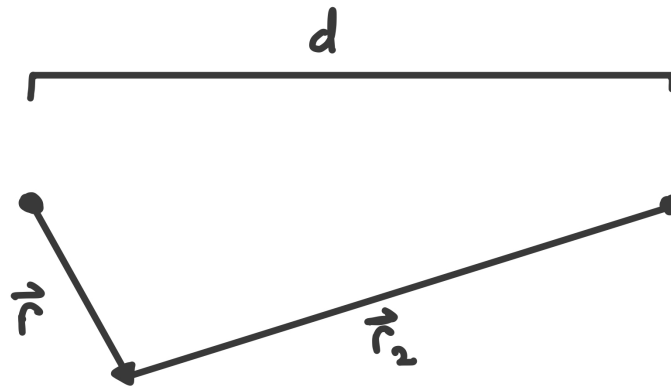


Figure 8: Geometric picture of the regime $r \ll d$ expanded near defect 1

The way we rewrite these coordinates is not too dissimilar from the previous two sections, and as before comes directly from the geometry of the configuration.

$$\frac{1}{r_2} = \frac{1}{\sqrt{r^2 + d^2 - 2rd\cos\theta}}$$
$$\sin\theta_2 = \frac{r\sin\theta}{\sqrt{r^2 + d^2 - 2rd\cos\theta}}$$
$$\cos\theta_2 = \frac{r\cos\theta - d}{\sqrt{r^2 + d^2 - rd\cos\theta}}$$

Applying our approximation yields:

30

$$\frac{1}{r_2} \approx \frac{1}{d}\left(1 + \frac{r}{d}\cos\theta\right)$$

$$\sin\theta_2 \approx \frac{r}{d}\sin\theta$$

$$\cos\theta_2 \approx -1$$

Unlike in the previous two sections the two defects are no longer on equal footing in this treatment, so our choice of defect signs does matter to the result that we obtain. We do want to understand the director field close to a defect regardless of its sign, so we treat the two cases separately, starting with the case $q_1 = -\frac{1}{2}$.

In this case, the sines initially expand into the same form as the previous two sections, at which point we can substitute in the appropriate approximations.

The angular terms we get are:

$$\sin(3\theta_1 - \theta_2) \approx -\sin 3\theta - \frac{r}{d}\cos 3\theta \sin\theta$$

$$\sin(\theta_1 + \theta_2) \approx -\sin\theta + \frac{r}{d}\sin^2\theta$$

$$\sin(2\theta_1) = \sin(2\theta)$$

Now substituting these terms into the full equation yields:

$$\nabla^2\phi_c = \frac{5\epsilon}{4}\frac{1}{r^2}\sin 3\theta + \frac{\epsilon}{8}\frac{1}{rd}(5\sin 4\theta - \sin 2\theta) \tag{29}$$

We recognize the first term above as corresponding to the component of the Dzyaloshinskii solution which is linear in $\epsilon$. This is fully expected and gives us some confidence

that we have obtained the correct equation. The second term contains the influence of the second defect and it is what we will now focus on.

We can as before simply guess the form of the solution to the second term:

$$\phi_{c,-1} = \frac{\epsilon r}{8d}(A \sin 4\theta - B \sin 2\theta) \tag{30}$$

Plugging in and solving for the coefficients, we obtain

$$\phi_{c,-1} = \frac{\epsilon}{24} \frac{r}{d}(\sin 2\theta - \sin 4\theta) \tag{31}$$

Now we can examine the case where $q_1 = \frac{1}{2}$.

Expanding the sines similarly to previous sections we get the terms

$$\sin(\theta_1 + \theta_2) \approx -\sin\theta + \frac{r}{d}\cos\theta\sin\theta$$

$$\sin(3\theta_2 - \theta_1) \approx \sin\theta + 3\frac{r}{d}\cos\theta\sin\theta$$

$$\sin(2\theta_2) \approx -2\frac{r}{d}\sin\theta$$

which we then plug into the equation to yield:

$$\nabla^2\phi_c = -\epsilon\frac{3}{4}\frac{1}{r^2}\sin\theta + \epsilon\frac{3}{8}\frac{1}{rd}\sin 2\theta \tag{32}$$

Again, the first term is the first-order Dzyaloshinskii correction, and the second term is what we examine further, finding the solution:

32

$$\phi_{c,-1} = -\frac{\epsilon}{8}\frac{r}{d}\sin 2\theta \tag{33}$$

As in the previous section, we now need to take into account the isotropic contribution to the corrections we have just found.

This is simple enough to accomplish. Consider the isotropic component for defect 2:

$$\phi_{c,iso} = q_2\theta_2 = q_2 \arctan\left(\frac{r\sin\theta}{r\cos\theta - d}\right) \approx -\frac{r}{d}q_2\sin\theta$$

Thus, we now have a complete description for the director field close to one defect.

# 3    Results and Discussion

Having implemented a numerical method and having worked through the analytic approach to the extent possible, we are now prepared to apply these tools to understand some key behavior of the anisotropically-elastic system.

The two key things we study with these methods are the structure of the director field and how the strength of the interaction depends on epsilon. We will tackle each of these separately.

## 3.1    Structure of Director Field

The most straightforward of the three effects to examine is the structure of the director field. By this, we mean the subtle deviations from the isotropic solution, which

33

happen to be exactly the deviations we calculated analytically in the previous section. The analytic approximations constitute predictions which we wish to check against numerical results. While not a substitute for experiment, agreement between the two parallel approaches we have taken should lend some amount of credibility to our results since the two approaches have been independent since the derivation of Eq. 16.

Through the approximate analytical methods, we have picked out the most dominant deviations in the small-epsilon limit for four regions: far from both defects, near the midpoint of the two defects, and close to either defect. Each of these results has some dependence on $r$, as well as some angular dependence. The $r$-dependence for the most part defines the range of distances over which each approximation is valid, as higher-order terms will become significant at some point. We are thus most interested in the angular dependence, which in each approximation's region of validity will give us a sort of 'fingerprint' we can easily identify in the numerical results. We accomplish this by taking fourier transforms of $\phi - \phi_{iso}$ along specific circular loops in the computed director fields to pick out the angular components that give rise to the deviations.

Let us first examine the field far from both defects. In this regime, we expect strong peaks at frequencies of 1 and 3, with additional smoothly decreasing amplitudes at other frequencies, arising from the $\theta \cos \theta$ term. In figure 9 the angular components from the numerical result are shown. We see that these components appear to match qualitatively what we expect from the analytic result.

Now, close to the midpoint of the defects we expect just one strong peak at a frequency of 1. Repeating a similar procedure as above, figure 10 shows the angular components in this region of the numerical result. This result again appears to agree with the analytical approximation.
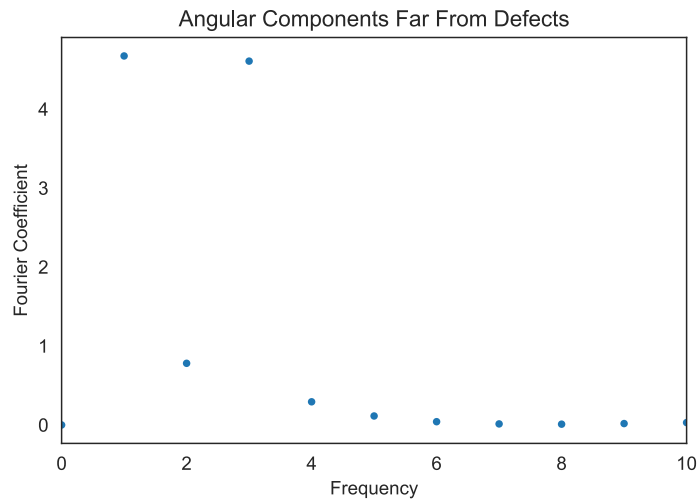
<center>34</center>

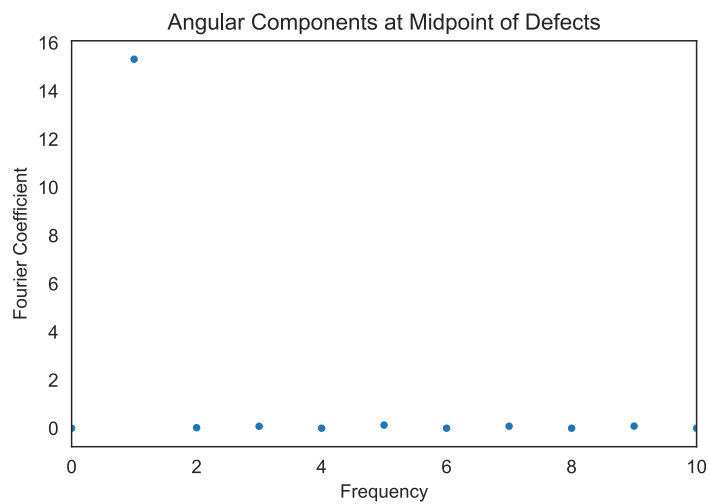Figure 9: Angular components of $\phi$ far from the defect pair.



Figure 10: Angular components of $\phi$ close to the midpoint of the defect pair.

35

Finally, we move onto the results near each defect. Near the negative defect we see in figure 12 that there are significant amplitudes at frequencies 1,2,3, and 4 as we expect from the analytic prediction, but we also see some contributions from higher frequencies. There are a couple of possible explanations for these. First, as they are fairly small they could be higher-order effects in either epsilon or $\frac{r}{d}$ not taken into account in our analysis. The other possibility is that these components arise effectively as noise from our method, as selecting points on a circle from a square lattice necessitates taking points at slightly different radii, an effect more prominent for smaller circles like the kind we must take for the analysis close to a defect. Either explanation would be consistent with the analytic prediction agreeing with our result.

Near the positive defect, we expect contributions at frequencies of 1 and 2, and in figure 11 this is what we see. Though the contribution at frequency 2 is relatively small, it is clearly present and somewhat larger than any higher frequency contribution. We again see a little bit of activity at some higher frequencies, which may be explained in the same way as for the negative defect.
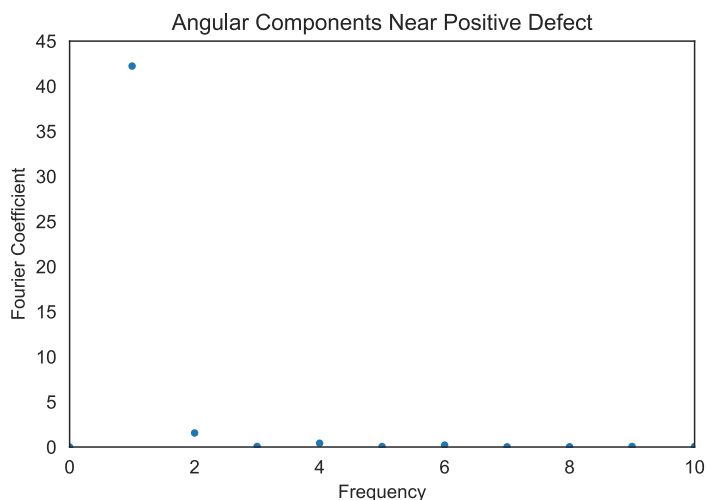


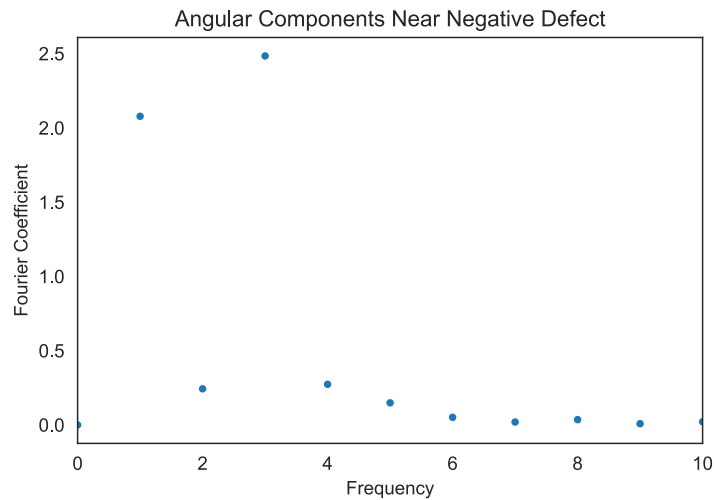Figure 11: Angular components of $\phi$ near the positive defect.

36

Figure 12: Angular components of $\phi$ near the negative defect.

## 3.2 Dependence of Interaction on $\epsilon$

Finally, we want to explore how the elastic anisotropy influences the strength of the interaction between the defects. Through our numerical work, we have at hand the capability to compute director fields across a range of anisotropies and defect separations. We can easily calculate the free energy of each of these director fields via numerical integration, (taking care as in the solution process to avoid the discontinuity inherent in $\phi$) then use the computed energies to approximate the derivative of the energy with respect to separation for a specific separation across a range of anisotropies. This derivative is of course the negative force between the defects, thus giving us a measure of the strength of the interaction.

Before diving in, let us briefly consider qualitatively what we might expect. We know that high anisotropies effectively allow one mode of distortion to store some of the total distortion required by the topological charge with little free energy penalty. Thus we expect that at either extreme in $\epsilon$ the strength of the interaction should be significantly lower than at more moderate values. Consequently, we also expect a

maximum in the interaction strength somewhere in these moderate values although we can't say *a priori* whether it should appear at $\epsilon = 0$ or at some other value. The location of the maximum should likely depend on the specific configuration of the defects including their orientations, as well as on some concept of how easily distortions of one mode can be rearranged into distortions of the other mode.

Now that we have a qualitative expectation, let's compute the numerical result. We choose our defect configurations to be as in figure 13 and compute configurations at separations of 380, 400, and 420 to obtain an approximation of the derivative at $d = 400$. As with all previous results, we take the system size to be of side length 1000 with 2000 lattice divisions in each dimension and set the defect core radius to be 3.
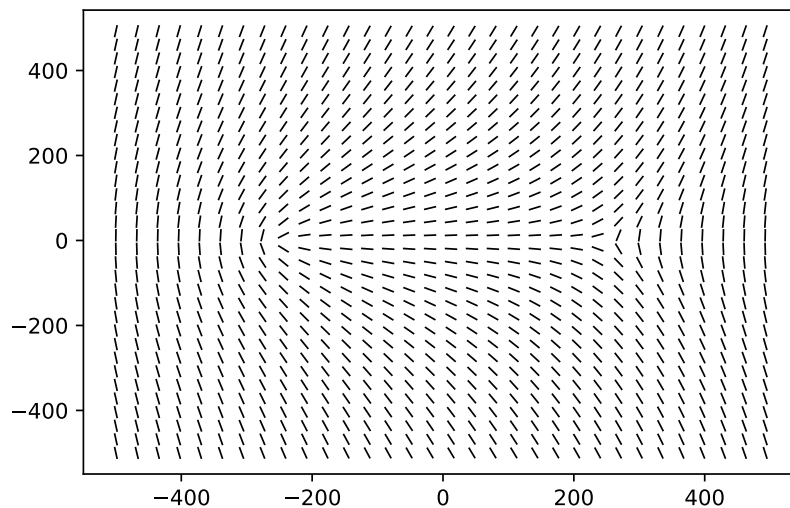


Figure 13: Illustration of the defect configuration used for the results in this section.

Figure 14 shows this numerical result, and we see immediately that it behaves in line with our qualitative expectation. The interaction strength is low at extreme anisotropies and has a maximum at a moderate anisotropy near $\epsilon = -0.2$. The location of the maximum is the most interesting part of the result, as it shows that

38

this specific defect configuration would be more favorable in a medium that has a slight positive anisotropy rather than a slight negative anisotropy.
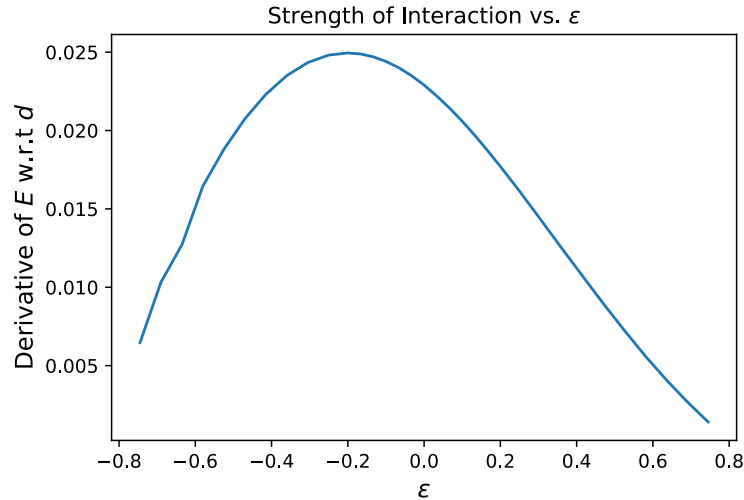


Figure 14: The (approximate) derivative of the interaction energy with respect to the defect separation, taken at a separation of 400.

For the defect configuration which has the opposite sides of the defects facing inwards, some early computational results of ours suggested that the interaction strength curve would be a reflection over $\epsilon = 0$ of the curve in figure 14, though time constraints disallowed us from running this case at full resolution to verify. If that result were to hold, these findings suggest that there is a different energetically-favorable defect configuration depending on the anisotropy of the medium. Therefore, in a real system where defects are free to rotate and move we would predict that the defects should rotate towards achieving this favorable configuration as they move towards each other to annihilate.

As a final note on the anisotropy-dependent interaction strength, we want to briefly demonstrate how the Peach-Koehler force breaks down. We of course expect from the nonlinearity of Eq. 16 that this description should not hold, but it warrants demonstration that even for small anisotropies it fails to be accurate.

39

For this we consider the corrections near a defect as found in section 2.3.3 to be the influence of the other defect, and then compute the stress and force using these correction fields. This stress is, if the PK approach were to be valid in this regime, the effective stress due to one defect at the location of the other defect, to first order in $\epsilon$. Working through from the definition of the PK force we find that

$$f_{PK} \propto \frac{\partial \phi_c}{\partial y}(1 + \epsilon) \tag{34}$$

Computing this for each of the two defects and neglecting the $\epsilon^2$ term that arises, we get:

$$f_{-+} \approx -\frac{1}{2}\left(\frac{1}{2} + \frac{3}{4}\epsilon\right) \tag{35}$$

$$f_{+-} \approx -\frac{1}{2}\left(\frac{1}{2} + \frac{5}{12}\epsilon\right) \tag{36}$$

In the above expressions we have dropped some constants, but the key takeaway is that the calculated force of the negative defect on the positive defect is not the same as the other way around. The two expressions only match for $\epsilon = 0$, where they give the same Peach-Koehler result as we found before. This asymmetry in the two forces now violates Newton's Third Law, demonstrating that we unfortunately can't use this very nice approach even for small elastic anisotropies.

# 4    Conclusion

To briefly conclude, the goal of this work was to gain insight into the behavior of interacting defects in anisotropically-elastic media. We accomplished this chiefly via a numerical approach, using a finite-difference relaxation method to compute direc-

tor fields for configurations of fixed defects. We supplemented this numerical work with approximate analytic methods to provide context and corroborate some of the numerical results. In the end we were able to find some details of the structure of the director field in various domains, demonstrate the invalidity of the Peach-Koehler force for anisotropically-elastic media, and find the dependence of the interaction strength on the degree of elastic anisotropy. This last result notably leads to a qualitative prediction about the dynamical behavior of defects in anisotropically-elastic media, i.e. that they should rotate to some preferred orientation with respect to one-another as they move towards annihilation.

41

# References

[1] P.M. Chaikin and T.C. Lubensky. *Principles of Condensed Matter Physics*. Cambridge University Press, 1995. Chap. 9.

[2] Steven D. Hudson and Edwin L. Thomas. "Frank Elastic-Constant Anisotropy Measured from Transmission-Electron-Microscope Images of Disclinations". In: *Physical Review Letters* (1989).

[3] Cheng Long et al. "Geometry and mechanics of disclination lines in 3D nematic liquid crystals". In: *Soft Matter* (2021). DOI: `10.1039/D0SM01899F`.

[4] Jonathan V. Selinger. *Introduction to the Theory of Soft Matter*. Springer, 2016. Chap. 10.